Improved thermochemical energy storage by steam addition during $CaCO_3$ decomposition: a kinetic approach

Juan Jesús Arcenegui Troya*,[1] *Pedro Enrique Sánchez-Jiménez*,[1] *Antonio Perejón*,[2,1] *Virginia Moreno,[2,1] José Manuel Valverde,[3] and Luis Allan Pérez-Maqueda*[1]*

[1] *Instituto de Ciencia de Materiales de Sevilla, C. S. I. C.-Universidad de Sevilla,*

C. Américo Vespucio nº 49, 41092 Sevilla, Spain

[2] *Departamento de Química Inorgánica, Facultad de Química, 41012 Universidad de Sevilla, Sevilla, Spain*

[3] *Departamento de Electrónica y Electromagnetismo, Facultad de Física, Universidad de Sevilla,*

Avenida Reina Mercedes s/n, Sevilla, 41012 Spain

(Dated: 18/12/2020)

Abstract

In the present work, we explore the use of steam in the $CaCO_3$ calcination step of a calcium looping process devised for integration into a thermochemical energy storage process (CaL-TCES). Steam produces a double benefit: firstly, it fastens the calcination, allowing a reduction of the temperature needed to attain full calcination in short residence times, as those required in practice, resulting in energy savings. This behaviour is justified on the bases of kinetic study results, as obtained from a non-parametric kinetic analysis, which demonstrates that the presence of steam during calcination can reduce the apparent activation energy from 175 kJ/mol to 142 kJ/mol with a steam's partial pressure of 29%. In addition, the results obtained for multicycle CaL-TCES tests show that steam alleviates the deactivation of the sorbent, which is one of the main limiting factors of this technology. This behaviour is explained in terms of the effect of steam on the microstructure of the resulting CaO. Importantly, the values of the residual conversion attained calcining in steam are higher than those without steam.

Keywords: Concentrated solar power; Limestone, Thermochemical energy storage; Calcium Looping; Steam; Kinetics

*Authors to whom correspondence should be addressed: jjarcenegui@icmse.csic.es, pedro.enrique@icmse.csic.es, aperejon@us.es, maqueda@icmse.csic.es

1. Introduction

Global warming is one of the most pressing challenges of our era. The global temperature has incremented by around 1.1-1.4 ^{o}C since pre-industrial times and this increment is mainly attributable to the greenhouse gases emissions [1]. Electricity production based on fossil fuels combustion accounts for a large share of these emissions, which urges for its replacement by renewable sources of energy. However, the intrinsic intermittency of some renewable energies, such as wind or solar, makes it difficult to match supply and demand continuously. The global deployment of low cost, efficient and environmentally friendly energy storage technologies is an avenue for overcoming this challenge. Specifically, Concentrated Solar Power (CSP) is a quickly growing technology that allows for the thermal energy storage (TES) in the form of sensible or latent heat, which enables the use of solar energy after sunset [2,3]. Commercial CSP plants do already use molten salts to store sensible heat that can be used overnight to generate electricity [3]. In latent heat storage systems, solar energy is stored in some materials when they undergo a phase change [4,5]. A third possibility under investigation is the thermochemical energy storage (TCES). The main advantages of TCES as compared to the two others are a significantly higher energy density and the possibility of long term storage [6].

Proposed integration of Thermochemical energy storage systems into CSP plants exploit solar power to drive a reversible endothermic reaction [7,8]. The reaction products are separately stored and they are brought back together to opportunely produce the reverse exothermic reaction when power supply is required. Advantageously, compared to TES, TCES provides significantly higher energy densities and the reaction by-products can be stored indefinitely in stable forms with negligible thermal losses [6]. In particular, TCES based on the reversible reaction between CaO and CO_2, referred as calcium-looping (CaL), stands out for the high energy density achievable (~ 3.2 GJ/m^3 as compared to 0.8 GJ/m^3 achieved by solar salts in the form of sensible heat), the low cost (10 ~€/ton) and the abundance of natural CaO precursors, such as dolomite and calcite. Other low cost and calcium rich materials such as steel or carbide slags, biomineralized $CaCO_3$ in natural byproducts have also been explored as possible CaO precursors [9,10]. Although CaL was originally proposed for carbon capture and storage (CaL-CSS), in recent years the use of the CaL technology for TCES has received a great deal of interest due to its promising results [11–13]. The proposed integration scheme of CaL as a TCES system in CSP plants (CaL-TCES) requires calcination to be carried out in inert gas at around 750 ^{o}C, while carbonation is usually carried out at 850 ^{o}C in pure CO_2 [14,15]. A major challenge to facilitate the commercial deployment of this technology is the marked material deactivation along ensuing cycles. The loss of reactivity towards CO_2 is attributed to strong sintering leading to a significant loss of surface readily available for carbonation [16–18]. The harsh carbonation conditions worsen the problem as it is known that CO_2 strongly promotes sintering [18–20]. In addition, it has been observed that carbonations at high temperature under high CO_2 concentration yields the formation of a blocking layer on the particles' surface, which impedes CO_2 from reaching the inner volume of the particles, that remains essentially unreacted. This pore plugging mechanism and the reaction-induced sintering of the surface layer constitute the main mechanisms of deactivation in TCES conditions [21–23]. Reducing the temperature of calcination is thus an important objective in the development of the technology, as the calcination temperature strongly conditions the design of the plants, including the size

of the calciner, the extension of the heliostat field, the number of collectors as well as the radiative losses [24–26]. Moreover, a decrease in the temperature needed for calcining limestone in the short residence times required in practise would result in significant energy savings. The recent proposal of flash calcination in vertical tube furnaces also demands rapid calcinations [27,28]

The speed-up effect of steam on $CaCO_3$ calcination has also been considered as a way to attain such reduction [29,30]. However, there is no consensus in the literature on the reasons for this acceleratory effect. For instance, Li et al. attributed it to an increase in the heat transfer coefficient [31–33], whereas other authors have pointed out a catalytic effect of H_2O as responsible [34–36]. The catalytic mechanism is usually rationalized in the higher affinity of H_2O molecule for active CaO sites, resulting in a displacement of CO_2 through the formation of a $Ca(OH)_2$ intermediate [30]. However, while that might be reasonable at moderate temperatures, it would be debatable at high temperatures, beyond the maximum stability of $Ca(OH)_2$. Alternatively, the formation of hydrogen carbonate ions as intermediates has also been suggested [37]. Finally, MacIntire and Stansel ascribed the faster calcination to changes induced in the crystal growth and surface reaction [38].

Besides the acceleration of the calcination reaction, it has been demonstrated that steam injection is an avenue for increasing the CO_2 uptake of CaO, regardless steam is injected during calcination, carbonation or at both stages [39–42]. The reason for the improvement has not yet been clarified but it might be related to the microstructure of the nascent CaO. Some authors have reported that steam enhances sintering, consequently reducing porosity but creating a more stable sorbent [42]. However, researchers have also observed otherwise; that steam injection alleviates sintering and reactivates CaO, thereby increasing its CO_2 capture capacity [40,43,44]. The lack of consensus might be attributed to the experimental conditions used, as the reversible CaO carbonation reaction is extremely sensitive to thermodynamical equilibrium [45]. Thus, the influence of water content surely depends on the temperature and CO_2 partial pressure used. So far, the improvement in CO_2 uptake has been demonstrated in works that attempt to simulate CO_2 capture from post-combustion gases in industrial plants. In carbon capture and storage conditions (CaL-CCS), calcination is carried out in about 70% CO_2. Therefore, high temperatures over 925ºC are necessary to overcome the equilibrium temperature.

In the present work, we explore the use of water steam to promote calcination, considering operation schemes compatible with thermochemical energy storage applications. Under such conditions, calcination is carried out in inert gas at about 750 ºC, a much lower temperature as compared to CaL-CCS. Herein, we study the behaviour of the system when a mixture steam-N_2 is used instead during the calcination stage with the aim of attaining the maximum feasible reduction in the calcination temperature.

Moreover, a kinetic approach is used to gain understanding of the influence of steam in promoting $CaCO_3$ calcination. The analysis is carried out by means of the non-parametric kinetics (NPK) method, which has demonstrated its capability to extract the kinetic parameters from experimental data without the previous assumption of a kinetic model, thereby avoiding bias in the analysis. [46,47] .

2. MATERIALS AND METHODS

The limestone used in this work (ESKAL 60) was supplied by KSL Staubtechnik GmbH (Germany). Figure 1. a) shows a micrograph of the particles. The particle size distribution (PSD) was determined by laser diffraction as described in [48]; the result is plotted in Fig.1.b). The sample exhibits a narrow PSD with a maximum approximately at 60 μm. Particles' size can strongly affect the kinetics of calcination and carbonation, as well as the multicycle performance of the sample [49,50].

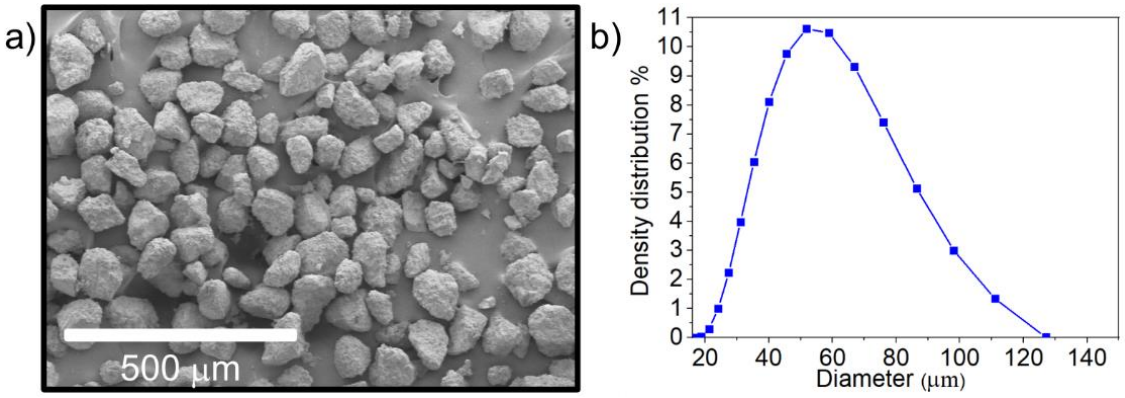

FIG 1: a) SEM micrographs of a sample of limestone used in this work. b) Particle size distribution.

Figure 2 shows a scheme of the experimental setup used. The experiments were conducted in a thermogravimetric analyzer LINSEIS STA PT 1600. The system is customized to allow steam injections in the furnace. N_2 was used as a purge gas and to pressurise the water tank. The water flow to the vaporizer was controlled through a water flow controller (WFC) Bronkhorst Liqui-Flow L13V12, which allows controlling the flow with an accuracy of 1%. After evaporation, steam was mixed with nitrogen in the vaporizer, and the mixture was led to the furnace through a heated transfer line kept at 165 ^{o}C to avoid condensation (red line in Fig. 2). The flow of gases to the vaporizer was controlled by using mass flow controllers (MFC).

The multicycle activity of limestone was tested with and without steam addition during the calcination stage. The multicycle carbonation/calcination tests carried out under CaL-TCES conditions started with a heating ramp at 20 ^{o}C·min^{-1} from room temperature to 500 ^{o}C. Then, a mixture of steam and N_2, with different partial pressures of steam, was injected in the furnace while the temperature was kept constant during 30 min to make sure that the mixture N_2-steam was uniformly distributed in the furnace before the calcination stage started. The temperature was subsequently increased at 20 ^{o}C·min^{-1} up to the selected calcination temperature. At this point, the temperature was maintained constant for 10 min to carry out the calcination under isothermal conditions. Since for a given temperature the time required to attain full calcination depends on the steam's partial pressure, the calcination temperature of these experiments was set at the minimum necessary to achieve full calcination from the first cycle. For instance, without steam, a minimum of 730 ^{o}C was necessary to fully calcine the limestone in short

residence times as those required in practice (< 10 min). Conversely, with a steam's partial pressure of 29%, complete calcination can be attained at 680 ^{o}C in less than 10 min. The minimum values of temperature required as a function of steam's partial pressure are collected in table 1.

TABLE 1: Minimum temperatures needed to attain full calcination in less than 10 min, as a function of the partial pressure used.

Partial pressure of steam	Minimum temperature required
No steam	730 ^{o}C
3 %	700 ^{o}C
29 %	680 ^{o}C

At the end of the calcination stage, steam was removed from the furnace and temperature was raised to 850 ^{o}C at a constant rate of 20 ^{o}C·min^{-1} in an atmosphere of pure N_2. At 850 ^{o}C N_2 was replaced by CO_2 to initiate a 5 min-lasting carbonation stage. After carbonation, the temperature was decreased to 500 ^{o}C and the cycle was repeated 20 times.

The kinetics of calcination in steam was studied from isothermal tests. Three different partial pressures of steam were used, namely, 0%, 3% and 29%. The temperature of the furnace was raised, at a constant rate of 5 ^{o}C·min^{-1}, from room temperature to the target temperature of the isotherm and then kept constant throughout the whole calcination process. To ensure that the mixture steam-N_2 was uniformly distributed in the furnace when the temperature of the isotherm was reached, the mixture of gases started being continuously injected into the furnace once a temperature of 400 ^{o}C was reached. The temperature of the isotherms ranged from 570 ^{o}C to 640 ^{o}C. The experimental data were analysed using a non-parametric kinetic method (NPK) [46,47] To test the results of the NPK study, the kinetic parameters obtained were used to predict the results of non-isothermal experiments.

A scanning electron microscope (SEM) HITACHI S4800 was used to study the effect of calcination and carbonation on the surface of the samples. Before SEM analysis, the samples were gold-coated utilizing an Emitech K550 Telstar sputter-coating machine (30 s, 30 mA).

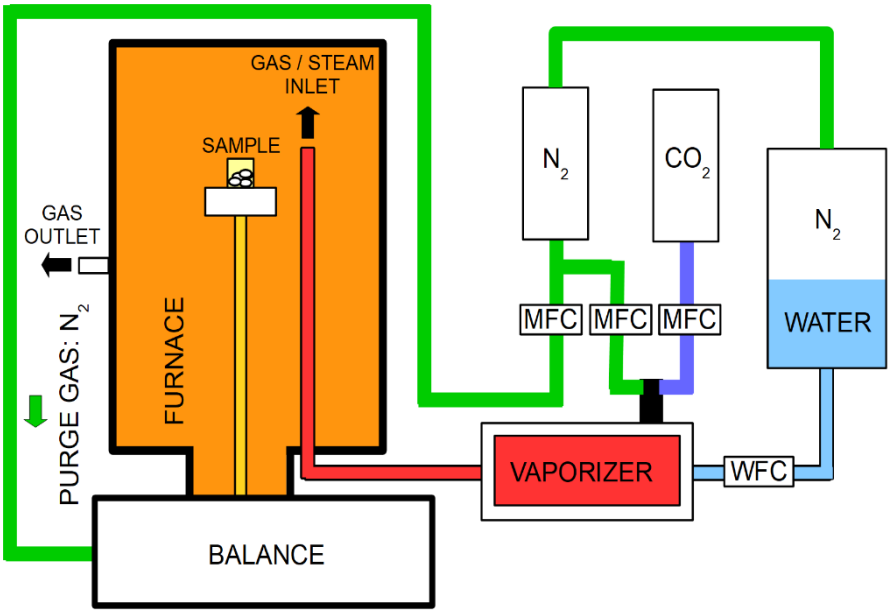

FIG. 2: Schematic illustration of the experimental setup.

3. RESULTS AND DISCUSSION

3.1. ISOTHERMAL CALCINATION OF $CaCO_3$ IN N_2/steam

Figure 3 shows the time evolution of the mass (%) during the calcination of limestone for three different steam's partial pressures at a temperature of 610 °C. The results are stoichiometrically consistent, as CaO accounts for 56% of the total mass of $CaCO_3$. The acceleratory effect of steam injection is clear and increases with the partial pressure of steam. The reaction is manifestly faster even with the lowest steam's partial pressure used.

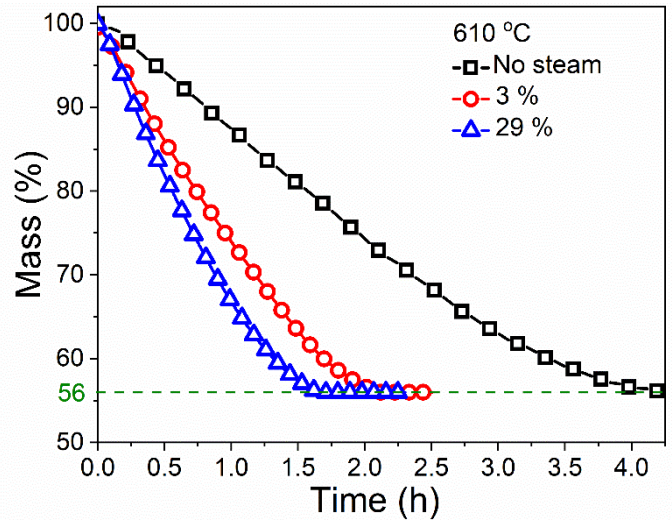

FIG. 3: Time evolution of the mass during the calcination of limestone, at 610 °C, for three different partial pressures of steam: 0 %, 3% and 29 %.

Figure 4 shows the SEM micrographs of the particles' surface after the isothermal calcination at 610 ºC. Figures a), b) and c) correspond to no steam, 3% and 29%, respectively. Steam's partial pressure has an evident impact on the surface of the nascent CaO. Samples calcined in the presence of steam exhibit a more open microstructure, which according to some authors would lower diffusional resistance to CO_2 and would result in higher values of conversion in the carbonation stage [40].

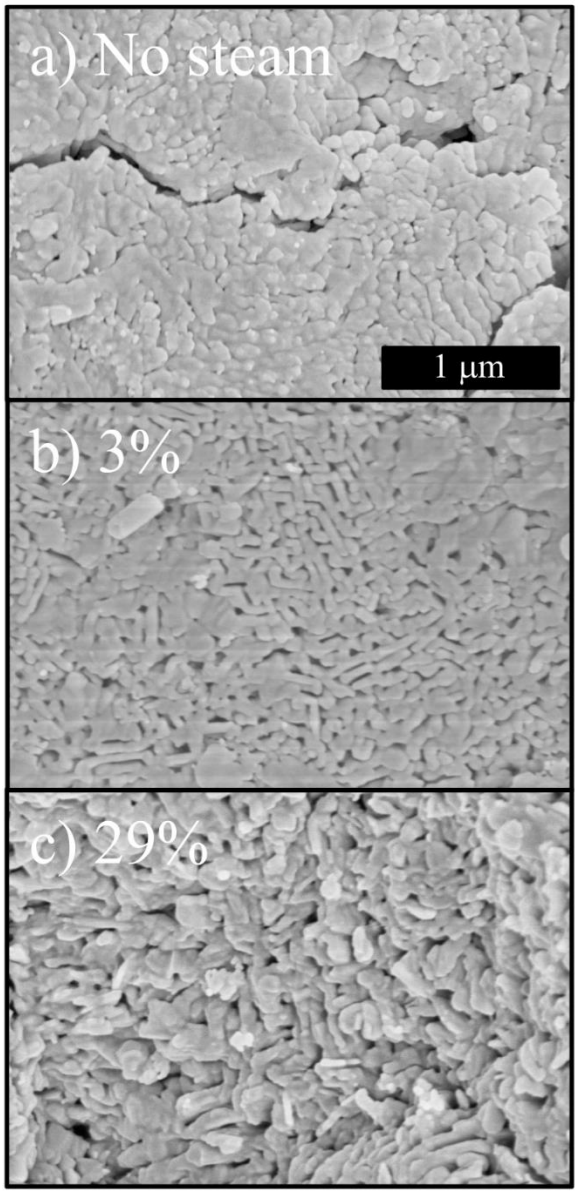

FIG. 4: SEM images of the particles' surface (CaO) taken after calcination at 610 ºC in steam with different partial pressures: a) No steam, b) 3%, c) 29%.

3.2. MULTICYCLIC EXPERIMENTS UNDER CaL-TCES CONDITIONS

Figure 5 shows the time evolution of the temperature and the mass during the second and nineteenth carbonation/calcination cycles when calcination stage is carried out at

700 °C, in a partial pressure of steam of 3%. The time interval during which steam was injected in the furnace is represented by a blue rectangle. As shown, the reactivity of the nascent CaO decreases with the cycle number due to pore plugging and sintering-induced deactivation. It has been widely reported that the carbonation stage is composed of two different phases. First, a fast kinetically-driven stage that corresponds to the carbonation reaction occurring on the surface of the particles, with a limited formation of bulk carbonate depending on the reaction conditions [51,52]. This is followed by a sluggish solid-state diffusion phase in which CO_2 diffuses across the $CaCO_3$ layer formed on the surface during the prior phase [16,53]. However, as previously reported, when the carbonation stage takes place in high CO_2 concentration at high temperature, the pore-plugging phenomena is dominant and, consequently, the extension of the diffusion stage is mostly negligible [14]. The apparent decrease in the mass during the ramp from 850 °C to 500 °C is an artificial buoyancy effect ascribed to changes in the density of the gas as a consequence of the abrupt temperature reduction.

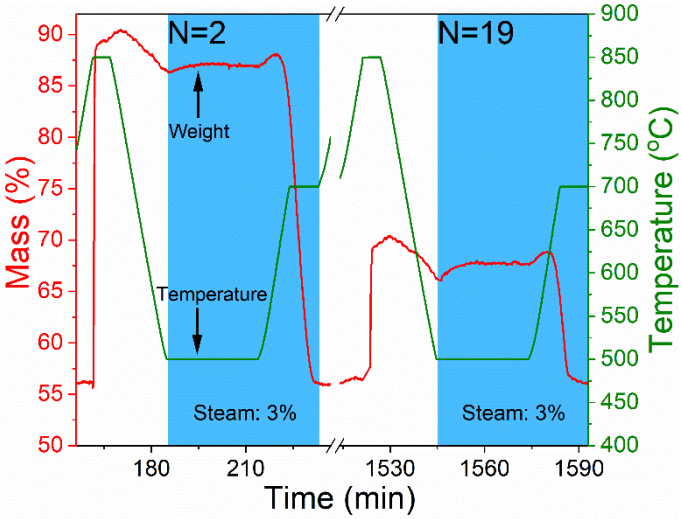

FIG. 5: Time evolution of the temperature and the mass during the second and nineteenth cycles carried out in TCES conditions. Calcination was driven at 700 °C with a steam's partial pressure of 3%.

Figure 6 shows the time evolution of the mass during calcination in the fifth cycle, at 700 °C under different steam fractions. Without steam, complete calcination of limestone cannot be attained in less than 10 min. Therefore, to achieve full calcination without steam in short residence times as those required in practice (<10min), the temperature needs to be increased at least up to 730 °C. However, the acceleratory effect of steam injection allows full calcination at 700 °C in less than 10 minutes.

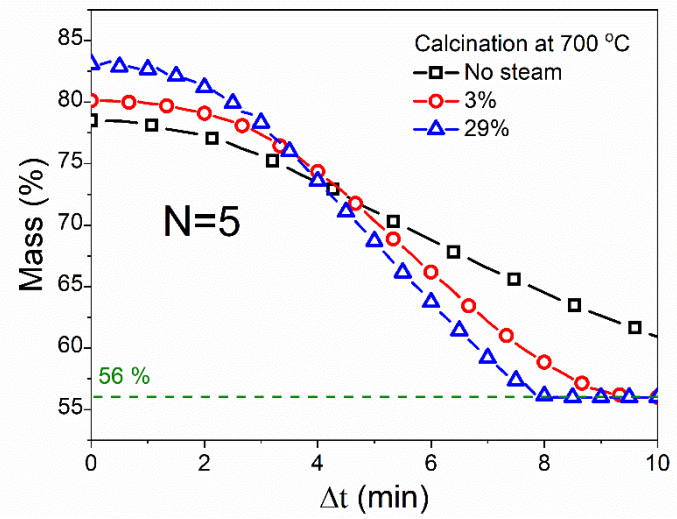

FIG. 6: Time evolution of the mass during calcination at the fifth cycle for the three values of steam's partial pressure used. The temperature of calcination was set at 700 °C in the three cases.

The multicycle effective conversion X_N at each cycle is calculated as the ratio of the mass of CaO converted to $CaCO_3$, to the total mass of the sample m before carbonation:

$$X_N = \frac{(m_N - m)\cdot W_{CaO}}{m\cdot W_{CO_2}} \tag{17}$$

Being m_N the sample mass after carbonation at the cycle N, and W_{CaO} and W_{CO_2} are the molar masses of CaO and CO_2, respectively. The evolution of the effective conversion with the carbonation/calcination cycle number are plotted in fig. 7. The temperature of calcination for each partial pressure of steam was set in such a way that complete calcination was attained in the first cycle, namely, 730 °C with no steam, 700 °C with 3% and 680 °C with 29%. This way, the performance of the material at the minimum attainable temperature can be compared. As evidenced in the plots, the injection of 3% steam has little influence in the multicycle performance despite the reduction of the minimum calcination temperature. Conversely, the higher steam volume injection has noticeable influence in the conversion, with an increase of about 50%. Data of conversion can be fitted using the following equation [54,55]:

$$X_N = X_r + \frac{X_1}{k(N-1)+(1-X_r/X_1)^{-1}} \tag{18}$$

Where X_r is the residual conversion, k the deactivation constant and X_1 the conversion at the first cycle. The fitting parameters are collected in Table 2.

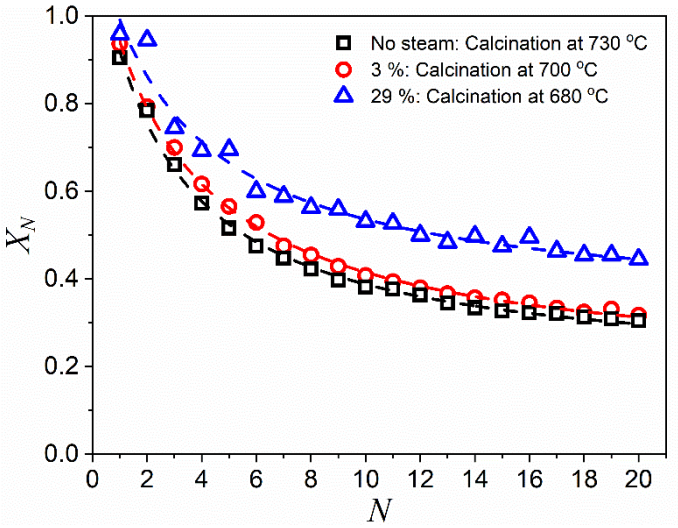

FIG. 7: Effective conversion as a function of the cycle number for the three steam's partial pressure used for calcination: 0 %, 3 % and 29 %.

Steam injection during carbonation improves the residual conversion, which is the most important parameter in practice, since the material is expected to be cycled hundreds of times.

TABLE 2: Best fitting parameters of equation (18) applied to the data presented in Figure 7.

Partial pressure of steam	X_r	k	R^2
No steam	0.18 ± 0.01	0.36 ± 0.02	0.996
3 %	0.18 ± 0.01	0.31 ± 0.01	0.999
29 %	0.32 ± 0.03	0.36 ± 0.07	0.969

One of the most striking conclusions of these results is the capability of reducing the minimum calcination temperature to achieve full decarbonation down to 680 °C for 29% steam. It is thus interesting to compare the multicycle performance at such temperature for all three steam volume concentration. Results are shown in Figure 8, which highlight the beneficial effect of steam. At such a low temperature, the multicycle performance of the sample calcined without steam is very poor, mainly because full calcination cannot be achieved.

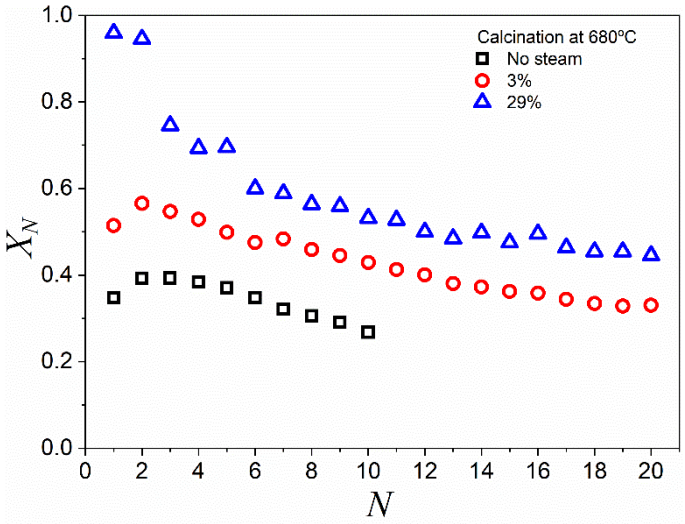

FIG. 8: Effective conversion as a function of the cycle number for samples calcined at 680ºC at the three steam's partial pressures.

Figure 9 shows the SEM images of the CaO particles' surface after the twentieth calcination, and the morphology of the $CaCO_3$ particles obtained after the twentieth carbonation for samples calcined without steam and with 29% of steam. $CaCO_3$ surface appears strongly sintered, with large grain sizes. Conversely, the micrographs reveal that injection of steam during the calcination stage helps the formation of a more open microstructure of the nascent CaO, thereby preserving larger specific surface area and making the inner of the particles more accessible to CO_2. This would explain the enhanced effective conversion observed in the multicycle test carried out in the presence of steam.

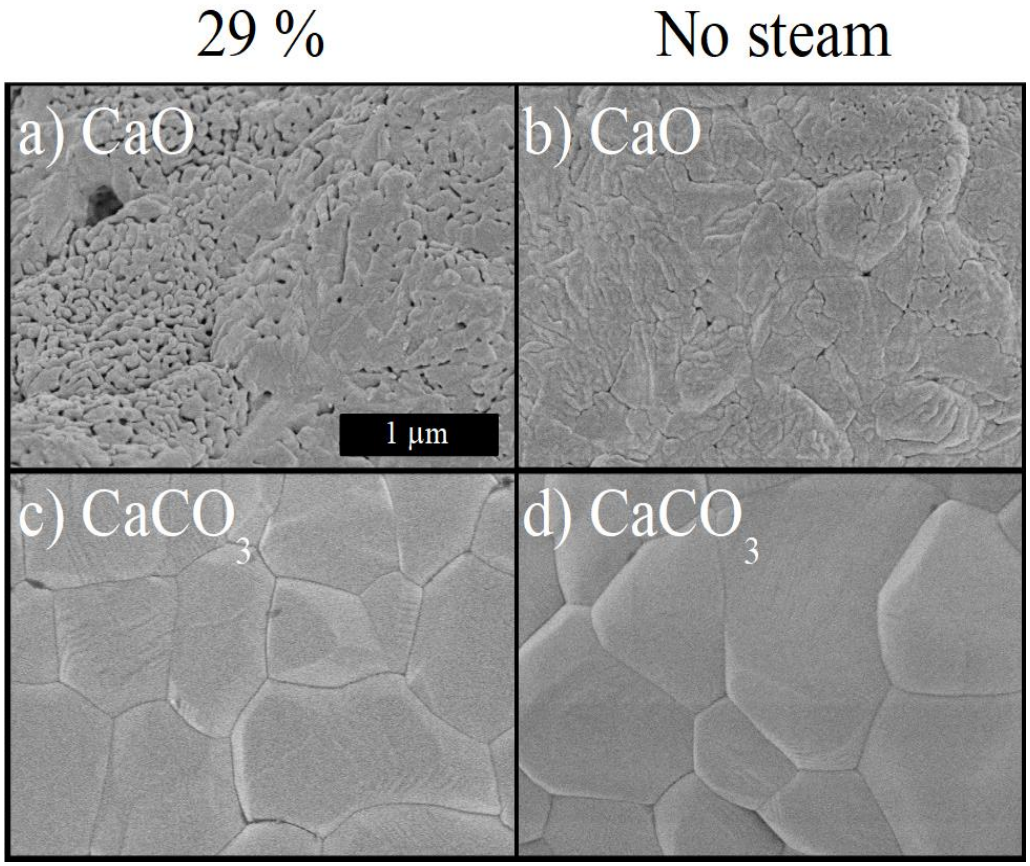

FIG. 9: SEM images of the particles' surface after the twentieth calcination and after the twentieth carbonation. a) CaO calcined with 29% steam, b) CaO calcined with no steam, c) CaO carbonated after calcination with 29% steamand d) CaO carbonation after calcination with no steam.

Figure 10 presents the effective conversion during the carbonation stage in the first cycle for the tests in which calcination was carried out at 680 °C. The three curves overlap up to the diffusion-controlled phase starts. Conversion during the diffusion phase is negligible; most mass is gained during the fast reaction-phase that occurs on the particle's surface. During this phase, a blocking layer of $CaCO_3$ is formed on the surface, while the inner remains more porous. This pore-plugging effect is shown in the SEM image in Fig. 11. A fracture on the particle's surface let us see the inner porous CaO core present underneath the $CaCO_3$ blocking layer. The smaller grain size evidences that the inner CaO does not undergo repeating carbonation and calcination as it is that responsible of the grain growth. The fact that the carbonation rate does not vary with steam concentration evidences that it does not truly depends on CaO morphology. The more porous structure displayed by CaO produced in steam results in larger reaction extension rather than in faster reactions. The mass gain curve during carbonation after calcining with 29% of steam (Fig. 10) also suggests improved carbonation during the diffusive stage, what can also be explained in terms of the more open morphology.

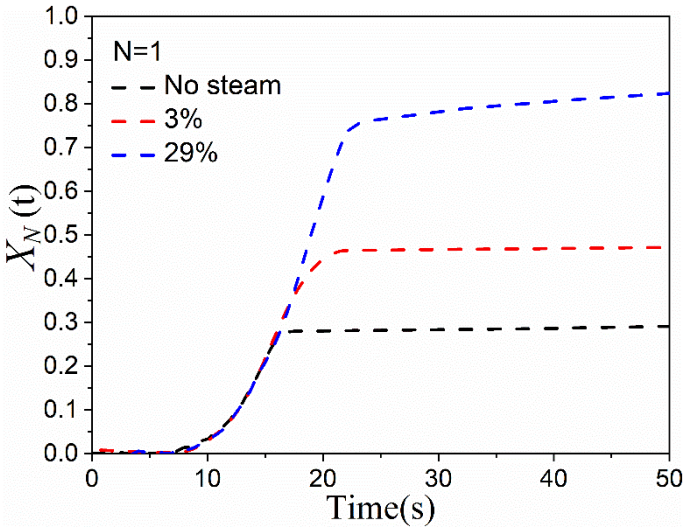

FIG. 10: Conversion during the carbonation stage in the first cycle of multicycle tests conducted with different values of steam's partial pressure. These data correspond to cycles in which calcination was carried out at 680 °C.

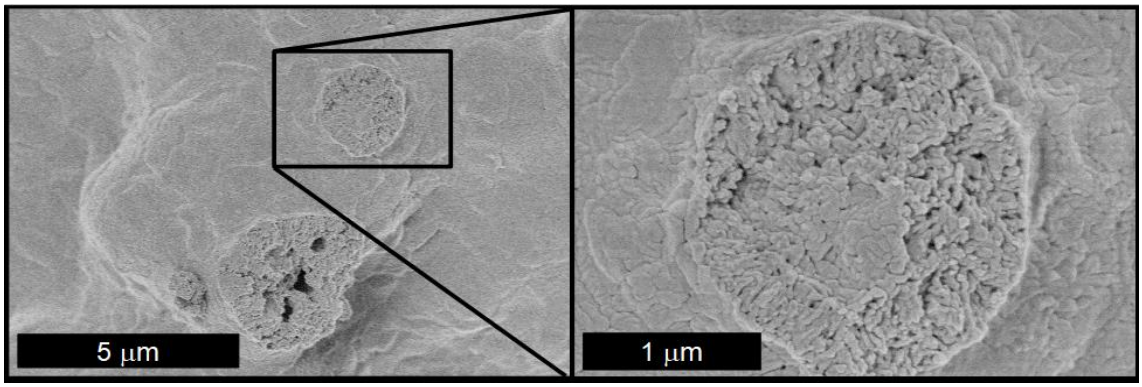

FIG. 11: SEM micrograph of particle's surface after calcination at 680 °C with no steam. The porous inner can be seen through an imperfection in its surface.

It is worth mentioning that several authors [56] have proposed the introduction of a hydration intermediate stage to reactivate spent CaO and enhance conversion. However, as shown here, it appears that a similar reactivation effect can be achieved by calcining in the presence of steam, without the need to introduce an additional process so that the steam injection during calcination could be considered an in-situ reactivation

3.3. KINETIC ANALYSIS OF ISOTHERMAL $CaCO_3$ CALCINATION

The kinetics of $CaCO_3$ calcination has been studied using a wide array of different methods, being the random pore model and shrinking core two of the most popular proposed for modelling the reaction [57]. However, the kinetic parameters published lack consistency, with activation energies ranging from 100 to 300 kJ/mol [58]. Besides experimental problems due to the strong influence of the reversible reaction [45,59], another explanation for the discrepancies might be the widespread use of model-fitting methods. Those methods rely on fitting experimental data to a list of assumed kinetic models. However, as it has been previously reported, goodness of fit does not suffice to claim a process obeys a given model, as experimental data might mathematically fit correctly any number of models yielding different activation energies and pre-exponential factors for each kinetic model used [60,61]. For this reason, many authors prefer model-free methods of kinetic analysis. Here, we employ the model-free Non Parametric Kinetic (NPK) analysis method to study the kinetics of $CaCO_3$ calcination in nitrogen, 3% and 29% of steam.

The kinetics of a solid-state reaction is typically described by:

$$d\alpha/dt = k(T) \cdot f(\alpha) \tag{1}$$

Where $k(T)$ is a function of temperature T and $f(\alpha)$ is a function of the extent of reaction α. Equation (1) can be integrated:

$$\int_{\alpha'=0}^{\alpha'=\alpha} d\alpha/f(\alpha) = \int_{t'=0}^{t'=t} dt'\, k(T) \tag{2}$$

Using the notation $g(\alpha) = \int_{\alpha'=0}^{\alpha'=\alpha} d\alpha/f(\alpha)$, integrating the right side of the equation for isothermal conditions ($T = constant$) and arranging conveniently, we get:

$$t = g(\alpha) \cdot (k(T))^{-1} \tag{3}$$

The NPK method was devised to obtain $(k(T))^{-1}$ and $g(\alpha)$ with no assumptions about their functional forms [46,47].
To apply the NPK analysis, a set of isothermal experiments were carried out at different temperatures. Then, the values of time were arranged in a matrix according to the following procedure: Each column include the time values needed to attain certain extent of reaction at a given temperature. Therefore, all time values in a column correspond to the same experiment. Consequently, time values in the rows end up arranged in such a way that each correspond to the time needed to attain a given extent of reaction at different temperatures. A matrix was constructed for each partial pressure of steam. The following matrix, equation (4), is an example of how data are arranged. In this matrix, for instance, t_{23} is the time it takes to attain the extent of reaction α_2 in isothermal conditions at T_3.

$$\boldsymbol{t} = \begin{matrix} T_1 \downarrow \\ \end{matrix} \begin{matrix} T_2 \downarrow \\ \end{matrix} \begin{matrix} T_3 \downarrow \\ \end{matrix} \begin{pmatrix} t_{11} & t_{12} & t_{13} \\ t_{21} & t_{22} & t_{23} \\ t_{31} & t_{32} & t_{33} \end{pmatrix} \begin{matrix} \leftarrow \alpha_1 \\ \leftarrow \alpha_2 \\ \leftarrow \alpha_3 \end{matrix} \tag{4}$$

The NPK method is based on a singular value decomposition (SVD) [46,47]. Three matrices, $\mathbf{u}, \mathbf{w}$ and $\boldsymbol{v}$, are obtained after applying an SVD to the matrix $\boldsymbol{t}$. The product of these matrices is $\boldsymbol{t}$:

$$\boldsymbol{t} = \boldsymbol{u} \cdot \boldsymbol{w} \cdot \boldsymbol{v}^{\boldsymbol{T}} \tag{5}$$

The first columns of $\mathbf{u}$ and $\boldsymbol{v}$ are proportional to the values of $g(\alpha)$ and $(k(T))^{-1}$, respectively. In the case of the matrix given by equation (4), it can be written as:

$$u(\mathrm{i}, 1) \propto g(\alpha_i) \quad \text{with} \quad \mathrm{i} = 1{:}3 \tag{6}$$

$$v(\mathrm{j}, 1) \propto (k(T_j))^{-1}) \quad \text{with} \quad \mathrm{j} = 1{:}3 \tag{7}$$

And any value of time can be approximated by:

$$t_{ij} = u(\mathrm{i}, 1) \cdot w(1,1) \cdot v(\mathrm{j}, 1) \quad \text{with} \quad \mathrm{i,j} = 1{:}3 \tag{8}$$

Where $w(1,1)$ is the first diagonal entry of $\boldsymbol{w}$. Figure 12 shows the comparison between the experimental values of α, represented by symbols, and the values calculated using

an SVD, plotted as solid lines. The curve (t,α) has been built using the equation (8) to calculate the value of time that corresponds to each value of α. As it can be observed, there is near perfect agreement between the experimental data and the plots built from the SVD. This indicates that experimental values of time can be effectively expressed as the product of a function of temperature times a function of the extent of reaction, as the equation (3) states.

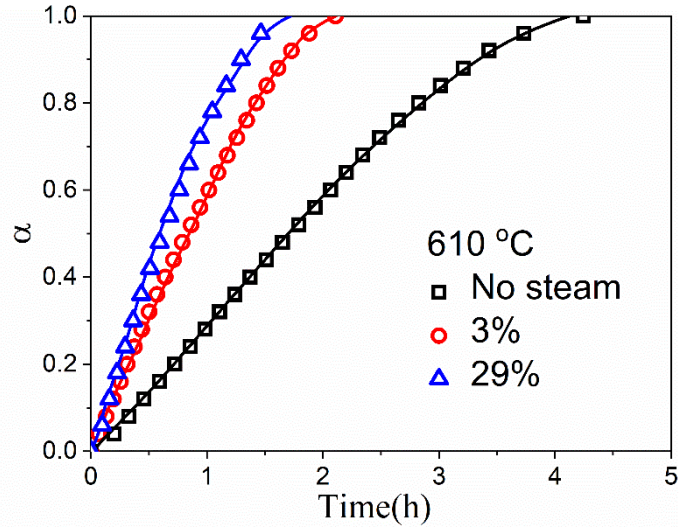

FIG. 12: Comparison between the experimental values of α calculated from isothermal decomposition experiments at 610 ºC and those obtained by means of the SVD method. The SVD was applied to data obtained with three different partial pressures of steam: 0%, 3% and 29%.

The values in the first column of $\boldsymbol{u}$, which are proportional to $g(\alpha)$, are plotted in Figure 13. Data have been normalized at $\alpha = 0.5$. Therefore, what is represented in Fig. 13 is $g(\alpha)/g(\alpha = 0.5)$. For the sake of clarity, the results for each steam's partial pressure have been first represented separately in fig. 13 a) to 13 c) and then all three together in fig. 13 d). All three curves overlap until α=0.6 (see Fig 13. d)), point at which the curve for 29 % deviates significantly. Fig. 13 also includes the theoretical functions $g(\alpha)/g(\alpha = 0.5)$ corresponding to the two kinetic models that most closely resemble the experimentally derived, namely, the Avrami-Erofeyev model (n=2, A2) and the contracting area model (R2). Other authors have previously reported these models to describe the calcination of $CaCO_3$ [58]. It is worth noting that the curves in Figure 13 are in- between those corresponding to the two ideal models, A2 and R2. This is not surprising, considering that the ideal models have been proposed assuming ideal conditions in terms of particle shape and size and driving forces for the process, while non-ideal systems, as the one studied here, suffer from deviations from ideality.
The dependence on temperature is assumed to be given by the Arrhenius equation:

$$k(T) = A \cdot e^{-E_a/RT} \tag{9}$$

Being A the pre-exponential factor, E_a the apparent activation energy and R the gas constant. Equations (7) and (9) can be combined to write:

$$1/v(T) = C \cdot e^{-E_a/RT} \tag{10}$$

Where $v(T)$ represents the first column of $\boldsymbol{v}$ and C is a constant of proportionality. Taking the natural logarithm of this expression:

$$ln(1/v(T)) = lnC - E_a/RT \tag{10}$$

Values of $ln(1/v(T))$ as a function of $1/T$ are plotted in figure 14. To each value of the steam's partial pressure corresponds a set of points; one point per each isothermal calcination experiment. Best fitting lines are also shown in the chart. The value of the apparent activation energy for each partial pressure can be calculated from the slope of these lines according to equation (10). Values of E_a obtained are given in the legend.

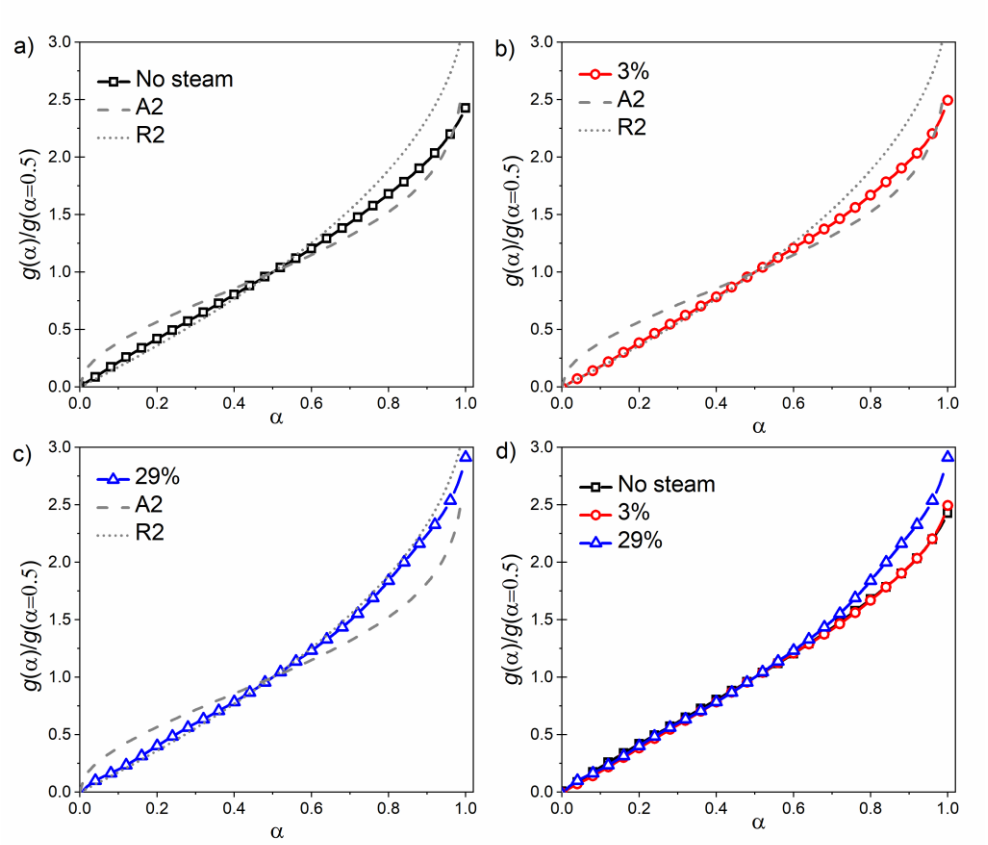

FIG. 13: Normalized values from the first column of $\boldsymbol{u}$ versus the extent of reaction, for the three different partial pressures of steam used: a) No steam, b) 3%, c) 29%. The results obtained with the three values of partial pressure are plotted together in d).

The value of activation energy obtained for the sample calcined without steam is in good agreement with the values reported in the literature [58]. Activation energy decreases from (175 ± 12) kJ/mol, with no steam, up to (142 ± 12) kJ/mol, with a steam's partial pressure of 29%. Giammaria et al. reported a similar reduction of activation energy in experiments conducted in a fixed bed reactor [37]. Activation energy, for calcination

with a partial pressure of 3%, has an intermediate value of (160 ± 4) kJ/mol. Thus, the addition of steam seems to induce a reduction on the activation energy for calcination.

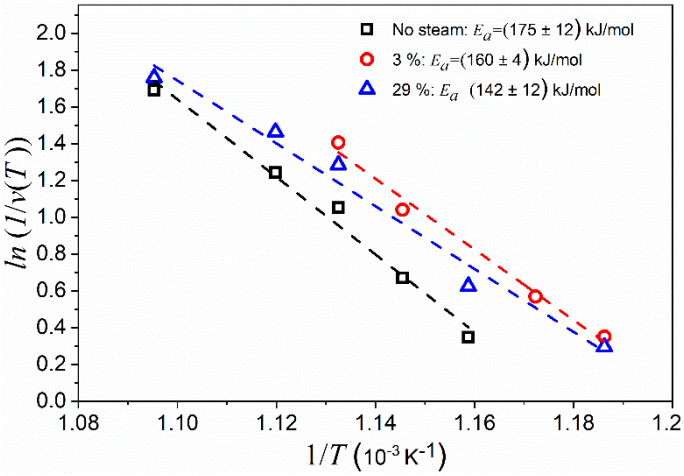

FIG. 14: Values of $ln(1/v(T))$ as a function of $1/T$. The values of apparent activation energy are given in the legend.

Combining equations (3), (6) and (9), the value of the time for a given extent of reaction can be written as:

$$t = (1/A^*) \cdot (u(\alpha)/u(\alpha = 0.5)) \cdot e^{E_a/RT} \tag{11}$$

Where $u(\alpha)/u(\alpha = 0.5)$ is the normalized function plotted in Fig. 13 and the new pre-exponential factor A^* is related to the pre-exponential factor A by:

$$A^* = A/g(\,\alpha = 0.5) \tag{12}$$

Values of E_a and $A^*$are collected in Table 3, where A^* has been calculated as the average of the values obtained for all temperatures. As can be observed, both factors decrease with the steam's partial pressure. While in principle a reduction on the pre-exponential factor might imply slower reaction kinetics, this is offset by the reduction of E_a. Actually, the decrease in the pre-exponential factor could be attributed to a kinetic compensation effect [62]. This simultaneous decrease of activation energy and pre-exponential factor was also observed by Wang et al. [30], who performed the kinetic analysis assuming an n order model, which according to recent results is not adequate for this reaction. The decrease in the activation energy has been rationalized in a change of the decomposition reaction pathway [37].

TABLE 3: Values of apparent activation energy and pre-exponential factor obtained for $CaCO_3$ calcination employing different partial pressures of steam.

Kinetic parameters		
Partial pressure of steam	E_a(kJ·mol^{-1})	A^*(s^{-1})
No steam	175 ± 12	$(3.4 \pm 0.1)\cdot 10^6$

3 %	160 ± 4	$(9.2 \pm 0.2)\cdot 10^5$
29 %	142 ± 12	$(1.1 \pm 0.4)\cdot 10^5$

The reconstruction of experimental curves using the kinetic parameters obtained in a kinetic analysis is the best avenue to test the reliability of the results. The curves used to feed the kinetic analysis cannot be used to validate the results obtained. Instead, the model and the kinetic parameters must be used to reconstruct data recorded in conditions different from those used in the kinetic analysis. To this end, non-isothermal calcination experiments run under constant heating rate were conducted. Then, the kinetic parameters in table 3 were used to simulate decomposition curves assuming those heating profiles.

The function $f(\alpha)$ in equation (1) can be calculated by differentiating $g(\alpha)$:

$$dg(\alpha)\ /d\alpha = (f(\alpha))^{-1} \tag{13}$$

Considering equations (9), (11) and (13), equation (1) can be rewritten as:

$$d\alpha/dt = A^* \cdot u(\alpha = 0.5) \cdot (du(\alpha)/d\alpha)^{-1} \cdot e^{-E_a/RT} \tag{14}$$

Therefore, integrating:

$$\int_{\alpha'=0}^{\alpha'=\alpha} d\alpha' = \alpha = \int_{t'=0}^{t'=t} dt' \cdot A^* \cdot u(\alpha = 0.5) \cdot (du(\alpha)/d\alpha)^{-1} \cdot e^{-E_a/RT(t')} \tag{15}$$

Here, the temperature is a function of time. In the case of a non-isothermal process, this integral can be approximated by a summation:

$$\alpha = \Delta t \cdot A^* \cdot u(\alpha = 0.5) \sum_i \ (du(\alpha)/d\alpha)^{-1}|_{\alpha_i} \cdot e^{-E_a/RT_i} \tag{16}$$

Where Δt is the time interval between two consecutive values of temperature (T_i and T_{i+1}) and α_i is the value of the extent of reaction when $T = T_i$. Equation (16) allows predicting the results of non-isothermal experiments using the kinetic parameters and the kinetic model obtained in isothermal conditions.

Figure 15 shows the time evolution of the extent of reaction during the calcination of limestone in experiments conducted at a constant heating rate of 5 ^{o}C/min. The lines represent the curves built using equation (16) and the kinetic parameters obtained with the NPK method. These curves fit reasonably well to the experimental data, which are plotted as symbols. The quality of the reconstruction is a proof of the validity of the kinetic parameters here obtained.

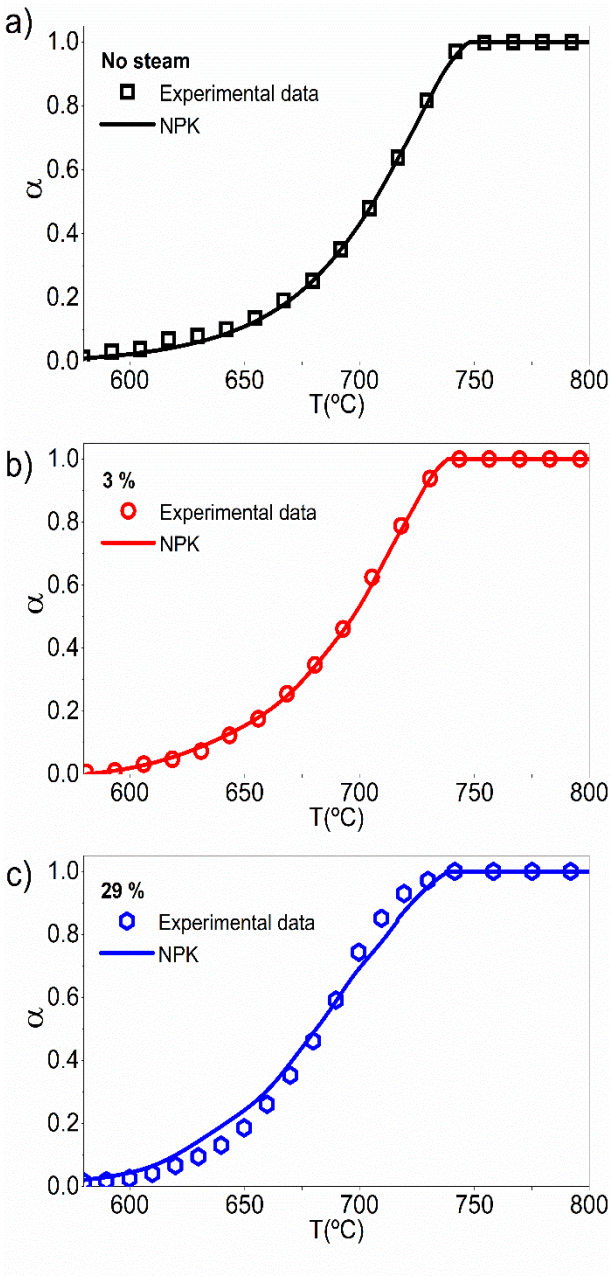

FIG. 15: Comparison among data from calcinations conducted at a linear heating ramp of 5 ºC/min and the values of α predicted using the kinetic parameters obtained with the NPK method: a) No steam, b) 3 % c) 29%.

4. CONCLUSIONS

The results herein obtained serves to clarify the accelerating effect of steam on the decomposition kinetics of $CaCO_3$ and it highlights the benefits gained by its addition during the calcination stage in CaL processes. It is shown how steam can be used to significantly reduce the effective calcination temperature of $CaCO_3$ while at the same time enhancing the multicycle activity. Steam promotion of $CaCO_3$ decomposition allows to attain effective calcination temperatures as low as 680 ºC with 29 % of steam. This would result in practice in important energy savings. In addition, multicycle

calcination/carbonation tests were carried out using a mixture N_2-water during calcination. These experiments evidence reduced CaO deactivation rate, what is ascribed to the strong influence steam has on the nascent CaO morphology. CaO regenerated in the presence of steam exhibits a less sintered microstructure and a more reactive surface that significantly promotes the subsequent carbonation. Consequently, the deactivation of the sorbent due to pore-plugging is minimized, resulting in residual conversion values about 50% higher than those attained without steam. The beneficial effects of water are dependent on steam concentration. Modest gains were observed using 3% steam but remarkable improvements when using 29% steam. Thus, calcination under steam is an in-situ reactivation that plays a role similar to ex-situ reactivation steps by hydration of CaO, without the need of introducing any additional processes.
The calcination rate enhancement was studied using a kinetic approach. Thus, the advanced non-parametric method, which does not require making any assumptions about the kinetic model, was used to study a set of calcination experiments run under isothermal conditions. The validity of the resulting kinetic parameters was proved not only by the reconstruction of the experimental curves used to carry out the analysis but by the accurate prediction of experimental curves recorded under different, non-isothermal, heating schedules. The kinetic analysis leads to the conclusion that the activation energy decreases from 175 kJ mol^{-1} to 142 kJ mol^{-1}, depending on the steam's partial pressure employed. This explains the reduction of the effective calcination temperature and is consistent with previous reports in which a catalytic effect is proposed to explain steam rate enhancement. Moreover, the ability of the NPK to provide an empirical model for the reaction, not restricted to a predetermined list, suggests that large amount of steam also modifies the kinetic model obeyed by the reaction.

Acknowledgements

This work has been supported by the Spanish Government Agency Ministerio de Economía y Competitividad (contracts CTQ2017-83602- C2-1-R and -2-R) and Junta de Andalucía-Consejería de Economía, Conocimiento, Empresas y Universidad-Fondo Europeo de Desarrollo Regional (FEDER) (Programa Operativo FEDER Andalucía 2014-2020, project US-1262507). We also acknowledge the funding received by the European Union's Horizon 2020 research and innovation programme under grant agreement No. 727348, project SOCRATCES.

References

[1] T. Knutson, J.P. Kossin, C. Mears, J. Perlwitz, M.F. Wehner, Ch. 3 Detection and Attribution of Climate Change, Forth Natioanl Clim. Assessment, Vol. I. (2017) 86. https://doi.org/10.7930/J01834ND.3.1.

[2] Lewis S. Nathan, Research opportunities to advance solar energy utilization, Science (80-.). 351 (2016) aad1920-1–9. https://doi.org/10.1126/science.aad1920.22.

[3] A. Palacios, C. Barreneche, M.E. Navarro, Y. Ding, Thermal energy storage technologies for concentrated solar power – A review from a materials perspective, Renew. Energy.

(2020). https://doi.org/10.1016/j.renene.2019.10.127.

[4] H. Nazir, M. Batool, F.J. Bolivar Osorio, M. Isaza-Ruiz, X. Xu, K. Vignarooban, P. Phelan, Inamuddin, A.M. Kannan, Recent developments in phase change materials for energy storage applications: A review, Int. J. Heat Mass Transf. (2019). https://doi.org/10.1016/j.ijheatmasstransfer.2018.09.126.

[5] M. Mehrali, J.E. ten Elshof, M. Shahi, A. Mahmoudi, Simultaneous solar-thermal energy harvesting and storage via shape stabilized salt hydrate phase change material, Chem. Eng. J. (2021). https://doi.org/10.1016/j.cej.2020.126624.

[6] P. Pardo, A. Deydier, Z. Anxionnaz-Minvielle, S. Rougé, M. Cabassud, P. Cognet, A review on high temperature thermochemical heat energy storage, Renew. Sustain. Energy Rev. 32 (2014) 591–610. https://doi.org/10.1016/j.rser.2013.12.014.

[7] C. Prieto, P. Cooper, A.I. Fernández, L.F. Cabeza, Review of technology: Thermochemical energy storage for concentrated solar power plants, Renew. Sustain. Energy Rev. 60 (2016) 909–929. https://doi.org/10.1016/j.rser.2015.12.364.

[8] A.J. Carrillo, J. González-Aguilar, M. Romero, J.M. Coronado, Solar Energy on Demand: A Review on High Temperature Thermochemical Heat Storage Systems and Materials, Chem. Rev. (2019). https://doi.org/10.1021/acs.chemrev.8b00315.

[9] A. Perejón, J.M. Valverde, J. Miranda-Pizarro, P.E. Sánchez-Jiménez, L.A. Pérez-Maqueda, Large-Scale Storage of Concentrated Solar Power from Industrial Waste, ACS Sustain. Chem. Eng. (2017). https://doi.org/10.1021/acssuschemeng.6b02576.

[10] J. Arcenegui-Troya, P.E. Sánchez-Jiménez, A. Perejón, J.M. Valverde, R. Chacartegui, L.A. Pérez-Maqueda, Calcium-Looping Performance of Biomineralized CaCO<inf>3</inf>for CO<inf>2</inf>Capture and Thermochemical Energy Storage, Ind. Eng. Chem. Res. 59 (2020). https://doi.org/10.1021/acs.iecr.9b05997.

[11] F. Raganati, R. Chirone, P. Ammendola, Calcium-looping for thermochemical energy storage in concentrating solar power applications: Evaluation of the effect of acoustic perturbation on the fluidized bed carbonation, Chem. Eng. J. (2020). https://doi.org/10.1016/j.cej.2019.123658.

[12] Y. Da, Y. Xuan, L. Teng, K. Zhang, X. Liu, Y. Ding, Calcium-based composites for direct solar-thermal conversion and thermochemical energy storage, Chem. Eng. J. (2020). https://doi.org/10.1016/j.cej.2019.122815.

[13] C. Tregambi, P. Salatino, R. Solimene, F. Montagnaro, An experimental characterization of Calcium Looping integrated with concentrated solar power, Chem. Eng. J. (2018). https://doi.org/10.1016/j.cej.2017.08.068.

[14] B. Sarrion, J.M. Valverde, A. Perejon, L. Perez-Maqueda, P.E. Sanchez-Jimenez, On the Multicycle Activity of Natural Limestone/Dolomite for Thermochemical Energy Storage of Concentrated Solar Power, Energy Technol. (2016). https://doi.org/10.1002/ente.201600068.

[15] R. Chacartegui, A. Alovisio, C. Ortiz, J.M. Valverde, V. Verda, J.A. Becerra, Thermochemical energy storage of concentrated solar power by integration of the calcium looping process and a CO2 power cycle, Appl. Energy. (2016). https://doi.org/10.1016/j.apenergy.2016.04.053.

[16] J.C. Abanades, D. Alvarez, Conversion limits in the reaction of CO2 with lime, Energy and Fuels. (2003). https://doi.org/10.1021/ef020152a.

[17] C. Salvador, D. Lu, E.J. Anthony, J.C. Abanades, Enhancement of CaO for CO2 capture in

an FBC environment, Chem. Eng. J. (2003). https://doi.org/10.1016/j.cej.2003.08.011.

[18] P.E. Sanchez-Jimenez, J.M. Valverde, L.A. Perez-Maqueda, Multicyclic conversion of limestone at Ca-looping conditions: The role of solid-sate diffusion controlled carbonation, Fuel. (2014). https://doi.org/10.1016/j.fuel.2013.09.064.

[19] R.H. Borgwardt, Calcium Oxide Sintering in Atmospheres Containing Water and Carbon Dioxide, Ind. Eng. Chem. Res. 28 (1989) 493–500. https://doi.org/10.1021/ie00088a019.

[20] M. Benitez-Guerrero, J.M. Valverde, A. Perejon, P.E. Sanchez-Jimenez, L.A. Perez-Maqueda, Effect of milling mechanism on the CO2 capture performance of limestone in the Calcium Looping process, Chem. Eng. J. 346 (2018) 549–556. https://doi.org/10.1016/j.cej.2018.03.146.

[21] M. Benitez-Guerrero, J.M. Valverde, P.E. Sanchez-Jimenez, A. Perejon, L.A. Perez-Maqueda, Multicycle activity of natural CaCO3 minerals for thermochemical energy storage in Concentrated Solar Power plants, Sol. Energy. 153 (2017) 188–199. https://doi.org/10.1016/j.solener.2017.05.068.

[22] M. Benitez-Guerrero, B. Sarrion, A. Perejon, P.E. Sanchez-Jimenez, L.A. Perez-Maqueda, J. Manuel Valverde, Large-scale high-temperature solar energy storage using natural minerals, Sol. Energy Mater. Sol. Cells. (2017). https://doi.org/10.1016/j.solmat.2017.04.013.

[23] P.E. Sánchez Jiménez, A. Perejón, M. Benítez Guerrero, J.M. Valverde, C. Ortiz, L.A. Pérez Maqueda, High-performance and low-cost macroporous calcium oxide based materials for thermochemical energy storage in concentrated solar power plants, Appl. Energy. (2019). https://doi.org/10.1016/j.apenergy.2018.10.131.

[24] X. Peng, M. Yao, T.W. Root, C.T. Maravelias, Design and analysis of concentrating solar power plants with fixed-bed reactors for thermochemical energy storage, Appl. Energy. 262 (2020) 114543. https://doi.org/10.1016/j.apenergy.2020.114543.

[25] A. Alovisio, R. Chacartegui, C. Ortiz, J.M. Valverde, V. Verda, Optimizing the CSP-Calcium Looping integration for Thermochemical Energy Storage, Energy Convers. Manag. (2017). https://doi.org/10.1016/j.enconman.2016.12.093.

[26] C. Ortiz, J.M. Valverde, R. Chacartegui, L.A. Perez-Maqueda, P. Giménez, The Calcium-Looping (CaCO3/CaO) process for thermochemical energy storage in Concentrating Solar Power plants, Renew. Sustain. Energy Rev. (2019). https://doi.org/10.1016/j.rser.2019.109252.

[27] SOCRATCES (SOlar Calcium-looping integRAtion for ThermoChemical Energy Storage);, (n.d.). https://socratces.eu/ (accessed November 23, 2020).

[28] C. Ortiz, J.M. Valverde, R. Chacartegui, L.A. Perez-Maqueda, Carbonation of Limestone Derived CaO for Thermochemical Energy Storage: From Kinetics to Process Integration in Concentrating Solar Plants, ACS Sustain. Chem. Eng. (2018). https://doi.org/10.1021/acssuschemeng.8b00199.

[29] R.M. McIntosh, J.H. Sharp, F.W. Wilburn, The thermal decomposition of dolomite, Thermochim. Acta. (1990). https://doi.org/10.1016/0040-6031(90)80228-Q.

[30] H. Wang, S. Guo, D. Liu, Y. Guo, D. Gao, S. Sun, A Dynamic Study on the Impacts of Water Vapor and Impurities on Limestone Calcination and CaO Sulfurization Processes in a Microfluidized Bed Reactor Analyzer, Energy and Fuels. (2016). https://doi.org/10.1021/acs.energyfuels.6b00456.

[31] Z.H. Li, Y. Wang, K. Xu, J.Z. Yang, S.B. Niu, H. Yao, Effect of steam on CaO regeneration, carbonation and hydration reactions for CO2 capture, Fuel Process. Technol. 151 (2016) 101–106. https://doi.org/10.1016/j.fuproc.2016.05.019.

[32] J. Yin, X. Kang, C. Qin, B. Feng, A. Veeraragavan, D. Saulov, Modeling of CaCO3 decomposition under CO2/H 2O atmosphere in calcium looping processes, Fuel Process. Technol. (2014). https://doi.org/10.1016/j.fuproc.2014.03.036.

[33] E.E. Berger, Effect of Steam on the Decomposition of Limestone, Ind. Eng. Chem. (1927). https://doi.org/10.1021/ie50209a026.

[34] D. Dollimore, T.L. Shively, W.A. Kneller, F.W. Wilburn, The thermal decomposition of dolomite samples, Proc. Conf. North Am. Therm. Anal. Soc., 26th. 165 (1998) 217–218.

[35] S. Guo, H. Wang, D. Liu, L. Yang, X. Wei, S. Wu, Understanding the Impacts of Impurities and Water Vapor on Limestone Calcination in a Laboratory-Scale Fluidized Bed, Energy and Fuels. 29 (2015) 7572–7583. https://doi.org/10.1021/acs.energyfuels.5b01218.

[36] Y. Wang, W.J. Thomson, The effects of steam and carbon dioxide on calcite decomposition using dynamic X-ray diffraction, Chem. Eng. Sci. (1995). https://doi.org/10.1016/0009-2509(95)00002-M.

[37] G. Giammaria, L. Lefferts, Catalytic effect of water on calcium carbonate decomposition, J. CO2 Util. 33 (2019) 341–356. https://doi.org/10.1016/j.jcou.2019.06.017.

[38] W.H. MacIntire, T.B. Stansel, Steam Catalysis in Calcinations of Dolomite and Limestone Fines, Ind. Eng. Chem. 45 (1953) 1548–1555. https://doi.org/10.1021/ie50523a050.

[39] F. Donat, N.H. Florin, E.J. Anthony, P.S. Fennell, Influence of high-temperature steam on the reactivity of CaO sorbent for CO 2 capture, Environ. Sci. Technol. (2012). https://doi.org/10.1021/es202679w.

[40] S. Champagne, D.Y. Lu, A. MacChi, R.T. Symonds, E.J. Anthony, Influence of steam injection during calcination on the reactivity of CaO-based sorbent for carbon capture, Ind. Eng. Chem. Res. (2013). https://doi.org/10.1021/ie3012787.

[41] V. Manovic, P.S. Fennell, M.J. Al-Jeboori, E.J. Anthony, Steam-enhanced calcium looping cycles with calcium aluminate pellets doped with bromides, Ind. Eng. Chem. Res. (2013). https://doi.org/10.1021/ie400197w.

[42] H. Guo, S. Yan, Y. Zhao, X. Ma, S. Wang, Influence of water vapor on cyclic CO2 capture performance in both carbonation and decarbonation stages for Ca-Al mixed oxide, Chem. Eng. J. (2019). https://doi.org/10.1016/j.cej.2018.11.173.

[43] Y. Wang, S. Lin, Y. Suzuki, Limestone calcination with CO2 capture (II): Decomposition in CO2/steam and CO2/N2 atmospheres, Energy and Fuels. 22 (2008) 2326–2331. https://doi.org/10.1021/ef800039k.

[44] M. Kavosh, K. Patchigolla, E.J. Anthony, J.E. Oakey, Carbonation performance of lime for cyclic CO2 capture following limestone calcination in steam/CO2 atmosphere, Appl. Energy. (2014). https://doi.org/10.1016/j.apenergy.2014.05.020.

[45] J.M. Criado, M. González, J. Málek, A. Ortega, The effect of the CO2 pressure on the thermal decomposition kinetics of calcium carbonate, Thermochim. Acta. (1995). https://doi.org/10.1016/0040-6031(94)01998-V.

[46] R. Serra, R. Nomen, J. Sempere, The non-parametric kinetics: A new method for the kinetic study of thermoanalytical data, J. Therm. Anal. Calorim. (1998). https://doi.org/10.1023/A:1010120203389.

[47] J. Sempere, R. Nomen, R. Serra, J. Soravilla, The NPK method an innovative approach for kinetic analysis of data from thermal analysis and calorimetry, Thermochim. Acta. (2002). https://doi.org/10.1016/S0040-6031(02)00037-0.

[48] H. Shi, R. Mohanty, S. Chakravarty, R. Cabiscol, M. Morgeneyer, H. Zetzener, J.Y. Ooi, A. Kwade, S. Luding, V. Magnanimo, Effect of particle size and cohesion on powder yielding and flow, KONA Powder Part. J. (2018). https://doi.org/10.14356/kona.2018014.

[49] J.D. Durán-Martín, P.E. Sánchez Jimenez, J.M. Valverde, A. Perejón, J. Arcenegui-Troya, P. García Triñanes, L.A. Pérez Maqueda, Role of particle size on the multicycle calcium looping activity of limestone for thermochemical energy storage, J. Adv. Res. (2020). https://doi.org/10.1016/j.jare.2019.10.008.

[50] H.J. Yoon, S. Mun, K.B. Lee, Facile reactivation of used CaO-based CO2 sorbent via physical treatment: Critical relationship between particle size and CO2 sorption performance, Chem. Eng. J. (2020). https://doi.org/10.1016/j.cej.2020.127234.

[51] G.A. Mutch, J.A. Anderson, D. Vega-Maza, Surface and bulk carbonate formation in calcium oxide during CO2 capture, Appl. Energy. (2017). https://doi.org/10.1016/j.apenergy.2017.05.130.

[52] Y.A. Criado, B. Arias, J.C. Abanades, Effect of the Carbonation Temperature on the CO2 Carrying Capacity of CaO, Ind. Eng. Chem. Res. (2018). https://doi.org/10.1021/acs.iecr.8b02111.

[53] R. Barker, The reversibility of the reaction CaCO3 ⇄ CaO+CO2, J. Appl. Chem. Biotechnol. (2007). https://doi.org/10.1002/jctb.5020231005.

[54] G.S. Grasa, J.C. Abanades, CO2 capture capacity of CaO in long series of carbonation/calcination cycles, Ind. Eng. Chem. Res. (2006). https://doi.org/10.1021/ie0606946.

[55] J.M. Valverde, P.E. Sanchez-Jimenez, A. Perejon, L.A. Perez-Maqueda, CO2 multicyclic capture of pretreated/doped CaO in the Ca-looping process. Theory and experiments, Phys. Chem. Chem. Phys. (2013). https://doi.org/10.1039/c3cp50480h.

[56] J. Blamey, V. Manovic, E.J. Anthony, D.R. Dugwell, P.S. Fennell, On steam hydration of CaO-based sorbent cycled for CO2 capture, Fuel. (2015). https://doi.org/10.1016/j.fuel.2015.02.026.

[57] A. Scaltsoyiannes, A. Lemonidou, CaCO3 decomposition for calcium-looping applications: Kinetic modeling in a fixed-bed reactor, Chem. Eng. Sci. X. (2020). https://doi.org/10.1016/j.cesx.2020.100071.

[58] L. Fedunik-Hofman, A. Bayon, S.W. Donne, Kinetics of solid-gas reactions and their application to carbonate looping systems, Energies. (2019). https://doi.org/10.3390/en12152981.

[59] B. V. L'Vov, Mechanism and kinetics of thermal decomposition of carbonates, Thermochim. Acta. (2002). https://doi.org/10.1016/S0040-6031(01)00757-2.

[60] C. Rodriguez-Navarro, E. Ruiz-Agudo, A. Luque, A.B. Rodriguez-Navarro, M. Ortega-Huertas, Thermal decomposition of calcite: Mechanisms of formation and textural evolution of CaO nanocrystals, Am. Mineral. (2009). https://doi.org/10.2138/am.2009.3021.

[61] P.E. Sánchez-Jiménez, L.A. Pérez-Maqueda, A. Perejón, J.M. Criado, Limitations of model-fitting methods for kinetic analysis: Polystyrene thermal degradation, Resour.

Conserv. Recycl. (2013). https://doi.org/10.1016/j.resconrec.2013.02.014.

[62] N. Koga, A review of the mutual dependence of Arrhenius parameters evaluated by the thermoanalytical study of solid-state reactions: The kinetic compensation effect, Thermochim. Acta. (1994). https://doi.org/10.1016/0040-6031(94)80202-5.